Turkish Journal of Chemistry

http://journals.tubitak.gov.tr/chem/

Research Article

Turk J Chem
(2019) 43: 475 – 491

doi:10.3906/kim-1807-7

Fuel characteristics and combustion behavior of seaweed-derived hydrochars

İsmail Cem KANTARLI[1,*], **Mehmet PALA**[2], **Yeliz YILDIRIM**[3], **Jale YANIK**[3], **Maria Helena ABREU**[4]

[1]Atatürk Medical Technology Vocational Training School, Ege University, İzmir, Turkey
[2]Department of Green Chemistry and Technology, Faculty of Bioscience Engineering, Ghent University, Ghent, Belgium
[3]Department of Chemistry, Faculty of Science, Ege University, İzmir, Turkey
[4]ALGAplus, Ílhavo, Portugal

Received: 03.07.2018 • **Accepted/Published Online:** 10.12.2018 • **Final Version:** 03.04.2019

Abstract: In this study, conversion of seaweeds into hydrochars was investigated with the aim of obtaining a renewable energy feedstock. The seaweeds *Fucus serratus* and *Alaria esculenta*, and a mixture of seaweeds, mainly consisting of *Cystoseria* sp. and *Laurencia* sp., were subjected to hydrothermal carbonization (HTC) in subcritical water at three different temperatures: 200, 225, and 250 °C. Fuel characteristics and chemical properties of the derived hydrochars were determined using the standard fuel analysis and spectroscopic methods. The combustion behavior of seaweeds and hydrochars was examined via nonisothermal thermogravimetric analysis under air atmosphere. The seaweed-derived hydrochar yields were lower than those of the lignocellulosic-derived hydrochar yields in the literature. Hydrochars derived from *Fucus serratus* and *Alaria esculenta* became increasingly similar to lignite with higher process temperature. *Fucus serratus*-derived hydrochars had the highest calorific value due to their higher carbon content and significantly lower ash content. HTC converted the seaweeds to hydrochars with improved combustion characteristics observed by lower burnout temperature and higher reactivity during combustion. The slagging index values of hydrochars implied medium or high slagging potential during combustion. On the other hand, HTC resulted in hydrochars with reduced fouling index implying medium fouling potential during their combustion due to the significant removal of alkali metals.

Key words: Hydrothermal conversion, seaweeds, hydrochar, combustion, slagging, fouling

1. Introduction

Depletion of fossil fuel resources that the world currently relies on requires the extensive production and utilization of sustainable and clean energy sources. One of these sources is biofuel, which is obtained from biomass. First-generation biofuels, bioethanol and biodiesel, obtained primarily from food crops, are currently the commercial bioenergy carriers of the world, but the global rise in food prices due to the intensive usage of food crops as feedstock for biofuel production fueled food vs. fuel debate and decreased the social acceptance of biofuels. This situation led to the development of second-generation biofuels produced from biomass resources that do not compete with agricultural food and feed production.[1]

Biofuels derived from marine biomass, particularly microalgae and seaweeds, have been considered to be a competitive alternative energy source which would eliminate the major drawbacks associated with first-generation biofuels by their ability to grow rapidly in water and avoiding the use of land. Macroalgae or

*Correspondence: ismail.cem.kantarli@ege.edu.tr

"seaweed" refers to macroscopic, multicellular, marine algae. They are plants that can grow in marine and fresh waters, achieving sizes up to 60 m. Their chemical composition is significantly different from that of terrestrial plants. They possess mainly carbohydrate structures in varying forms such as mannitol, laminarin, fucoidan, and alginic acid instead of lignocellulose.[2] Certain species of macroalgae are ideal candidates for the production of bioethanol as carbohydrates from macroalgae can be extracted to produce fermentable sugars.[3] On the other hand, microalgae are potential candidates for biodiesel production since they possess mainly lipids.[4]

Former studies in the literature reported the conversion of seaweeds into energy through biochemical routes such as fermentation to produce bioethanol and anaerobic digestion to produce gas.[5,6] On the other hand, recent studies on conversion of seaweeds into energy have also focused on thermochemical routes[7] such as combustion, pyrolysis, gasification, and hydrothermal conversion. For application of combustion, pyrolysis, or gasification, the high amounts of water and inorganics present in seaweeds are the major drawbacks since energy-consuming drying of seaweed is needed and slagging, fouling, and corrosion may occur during combustion and gasification due to the high amount of inorganic content.[2]

Hydrothermal conversion can eliminate these drawbacks since it does not need the drying of biomass before the process[8] and the water-soluble inorganics are removed during the process.[9] In the case of applying hydrothermal conversion to biomass in aqueous medium in the temperature range between 160 and 250 °C and at corresponding autogenic pressures up to approximately 2 MPa in a closed vessel, the process is named as hydrothermal carbonization (HTC). A carbon-rich solid product, named hydrochar, is obtained as the main product of HTC.[10]

In recent years, several authors have carried out HTC studies with a variety of biomass such as woody biomass,[11] agricultural wastes,[12] food wastes,[13] microalgae,[14] sludge,[15–18] and manure of different livestock.[19–21] Seaweeds could also be a good choice to produce carbon rich energy feedstocks by HTC method due to the advantage of processing wet biomass. Currently, there are a limited number of studies on HTC of seaweeds in the literature. Xu et al. studied HTC of *Sargassum horneri* at different temperatures (180–210 °C) in presence of catalyst (citric acid) for the reaction times between 2 and 16 h.[22] They observed that both the temperature and catalyst increased the carbon content of hydrochar obtained from *Sargassum horneri* by up to 46.8% and the calorific value by up to 25.1 MJ kg^{-1}.

Smith et al. studied the HTC of *Laminaria digitata*, *Laminaria hyperborea*, and *Alaria esculenta* at two temperatures (200 and 250 °C).[23] They observed that HTC of seaweeds typically produced hydrochar with improved calorific value and reduced ash content. They also investigated the fate of ash during HTC of *Laminaria hyperborea* at the same temperatures in another study.[24] They calculated predictive slagging and fouling indices of seaweeds and hydrochars in order to understand the influence of the ash chemistry on their combustion behavior. They observed a significant removal of the alkali metals, K and Na, and chlorine by HTC which would reduce the slagging and fouling during combustion of hydrochar.

The main objective of this study was to produce hydrochars by HTC of several seaweed species and to investigate the variation of the fuel characteristics, chemical properties, and combustion behavior of hydrochars with process temperature using different analytical methods including elemental analysis, Fourier transform infrared (FTIR) spectroscopy, and thermogravimetric analysis (TGA). In addition, slagging and fouling indices of hydrochars were calculated in order to predict combustion-related problems.

Three types of seaweed-origin feedstock were tested in the HTC experiments of this study. One of them was *Fucus serratus*, which is a species olive-brown in color and found along the Atlantic coast of Europe and

Northeast America. The other one was *Alaria esculenta*, which is brown in color and found along the coasts of the far North Atlantic Ocean. The third type was a mixture of seaweeds, mainly consisting of *Cystoseria* sp. and *Laurencia* sp. found along the Black Sea coast. Seaweed species will be denoted as FS, AE, and BS for *Fucus serratus*, *Alaria esculenta*, and mixed species *Cystoseria* sp. and *Laurencia* sp., respectively.

2. Results and discussion

2.1. Feedstock characteristics

Some properties of seaweeds used as feedstock in this study are presented in Table 1. Metal content of seaweeds determined by X-ray fluorescence spectroscopy were given in Table 2 as their respective oxides.

Table 1. Characteristics of seaweeds.

	AE	BS	FS
Proximate analysis, (wt.%)			
Moisture	5.8	8.6	7.7
Volatile matter	47.2	49.5	55.9
Ash	30.8	20.7	21.2
Fixed carbon	16.2	21.2	15.2
Ultimate analysis, (dry basis, wt.%)			
C	28.3	32.7	35.1
H	4.4	4.5	4.7
N	1.7	1.1	1.3
S	0.5	1.0	0.9
O*	34.3	40.0	36.8
Protein, (dry basis, wt.%)	10.6	6.9	8.1
Oil, (dry basis, wt.%)	0.6	1.3	1.5
HHV (MJ/kg)	10.8	12.1	13.5

*Calculated from difference.

As expected, seaweeds have high ash content, similar to other seaweeds reported in the literature.[7] The high chlorine (2.8–2.9 wt.%) and alkaline content (Ca, K, Mg, and Na) of seaweeds (Table 2) presents the potential of slagging and fouling during their combustion. The ultimate analysis shows that seaweeds had C and H contents lower than those of lignocellulosic biomasses in the literature.[21,25] Besides, seaweeds had higher N content (attributed to protein content) than lignocellulosic biomasses in the literature.

2.2. Hydrochar production

Hydrochar production was carried out at different temperatures (200–250 °C) with a seaweed/water ratio of 25% by weight for a reaction time of 30 min under autogenic pressure. The seaweed/water ratio was selected based on the original water content of seaweeds. The reaction time was optimized based on the preliminary experiments. The variations in hydrochar yields with temperature are shown in Figure 1. Hydrochar samples were defined as following the "Seaweed species–Temperature" sequence (e.g., AE-250 corresponds to hydrochar obtained from HTC of *Alaria esculenta* at 250 °C).

Table 2. Mineral composition in seaweeds (g mineral/100 g seaweed) by XRF spectroscopy prepared by the pressed pellet method.

	AE	**BS**	**FS**
Na_2O	7.96	4.35	6.88
MgO	0.76	0.89	0.72
Al_2O_3	0.58	0.18	0.15
SiO_2	1.95	0.33	0.07
P_2O_5	0.22	0.03	0.04
Cl	5.25	2.09	2.77
K_2O	4.91	2.55	2.88
CaO	1.83	3.77	1.03
TiO_2	0.03	< 0.01	< 0.01
MnO	0.01	< 0.01	< 0.01
Fe_2O_3	0.19	0.06	0.02
CuO	< 0.01	< 0.01	< 0.01

All values are dry weight % . Elements are represented as their respective oxides.

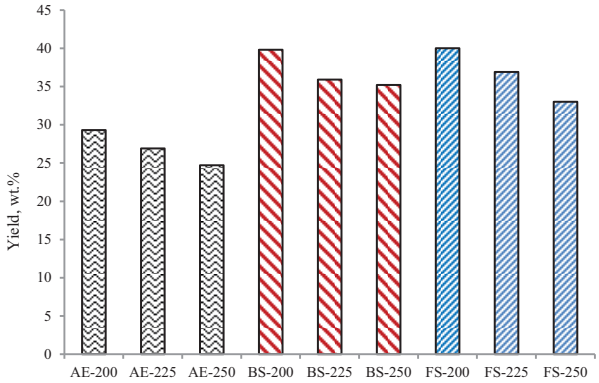

Figure 1. Hydrochar yields obtained from seaweeds at different temperatures (dry ash free basis) (wt.%).

A slight decrease in hydrochar yields with increasing of temperature was observed for all seaweed species. Temperature did not have much effect on the hydrochar yield in the range of 200–250 °C, which might be attributed to the high Ca content in seaweeds as suggested by Smith et al.[23] They suggested the possible role of calcium and magnesium present in the process waters in the formation of the char during HTC of macroalgae by nucleating alginate hydrolysis fragments and forming nuclei for growth of char, based on the study by Chen et al.[26] on HTC of an alginate. Smith et al. supported this theory by the metal analysis of the hydrochars, which showed the increase of calcium and magnesium content and absence of potassium and sodium content within the hydrochars in comparison with seaweeds. The effect of temperature on hydrochar yield was more significant in HTC of lignocellulosic biomass given in the literature. For example, the hydrochar yields ranged between 60% and 65% at low temperature HTC (200 °C) and between 45% and 53% at high temperature HTC (250 °C) for grape pomace, coconut fiber, and eucalyptus leaves.[25,27] It must be noted that similar hydrochar yields were reported for seaweeds in the study by Smith et al.[23] They obtained hydrochar yields of 30.0%,

21.8%, and 33.0% at 200 °C, and 23.7%, 18.4%, and 31.7% at 250 °C for *Alaria esculenta*, *Laminara digitate*, and *Laminara hyperborea*, respectively.

2.3. Fuel characteristics of hydrochars

Proximate, elemental, and energy analysis results of seaweed-derived hydrochars are presented in Table 3. Hydrochars had lower ash contents in comparison to feedstocks, which was due to the solubility of inorganics at subcritical water conditions.[25] Hydrochars derived from AE and BS had lower ash content by 18%–34% and by 21.7%–45.4%, respectively, than that derived from raw seaweeds. An extreme decrease in ash content was observed in the case of FS. FS-derived hydrochars had lower ash content by 85%–92% than that derived from raw FS, indicating high water solubility of inorganics in FS. Volatile matter contents of the resulting hydrochars were lower than those of seaweeds indicating the improvement of the carbon stability by HTC. Volatile matter content of the FS-derived hydrochars did not change with HTC temperature. On the other hand, volatile matter content of hydrochars derived from AE and BS decreased with increasing temperature indicating the further improvement of carbon stability in hydrochars.

Table 3. Proximate, elemental, and energy analyses of seaweed-derived hydrochars (dry basis).

Energy yield (%)	Proximate analysis, wt.%			Elemental analysis, wt.%					O/C	H/C	HHV [MJ/kg]	Energy densification	
	Ash	Volatile matter	Fixed carbon	C	H	N	S	O*					
AE-200	19.6	44.3	36.1	45.2	4.5	2.7	0.0	28.0	0.46	1.19	17.74	1.64	48.09
AE-225	24.0	41.0	35.0	45.8	4.1	2.5	0.2	23.5	0.39	1.08	17.80	1.64	44.35
AE-250	25.1	35.7	39.2	46.7	4.3	2.6	0.2	21.1	0.34	1.11	18.68	1.72	42.68
BS-200	11.3	46.3	42.4	48.2	4.3	1.6	0.1	34.5	0.54	1.07	18.09	1.50	59.53
BS-225	16.2	43.1	40.7	48.5	4.5	1.6	1.1	28.1	0.43	1.11	18.78	1.56	55.76
BS-250	15.6	37.0	47.4	47.9	4.2	1.5	0.2	30.7	0.48	1.04	18.14	1.51	52.81
FS-200	1.6	50.4	48.0	57.8	5.5	2.0	0.2	32.9	0.43	1.14	23.23	1.73	68.76
FS-225	1.8	49.9	48.3	62.4	5.5	2.5	0.3	27.5	0.33	1.06	25.32	1.88	69.18
FS-250	3.2	50.3	46.5	64.9	5.6	2.1	0.2	24.2	0.28	1.02	26.60	1.98	65.11

*Calculated from difference.

Hydrochars had higher carbon content in comparison with raw seaweeds, as expected. In the temperature range studied, carbon content of hydrochar did not significantly change (except FS). This result suggests that the majority of carbonization occurs at around 200 °C. Figure 2 represents the carbon distribution among the products during HTC. Carbon in gas product was determined by difference. HTC of seaweeds resulted in the 40%–50% of initial carbon remaining in the resulting hydrochar. With increasing temperature from 200 °C to 250 °C, the carbon content of the aqueous-phase slightly decreased while the carbon in the gas (mainly CO_2, data not shown) increased slightly (Figure 2), which could be due to the further degradation of organics in aqueous phase into gaseous compounds with the increase of temperature reported earlier.[25]

Van Krevelen diagram of hydrochars was drawn in order to assess the variation in the elemental composition of the materials (from seaweed to hydrochar) and also to get information on the reaction pathways (Figure 3). The evolution of the atomic O/C and H/C ratios is helpful in understanding the degree of deoxygenation of biomass by decarboxylation and/or by dehydration.[28] For comparison, typical ranges for anthracite, bituminous coal, and lignite are also shown in the diagram.

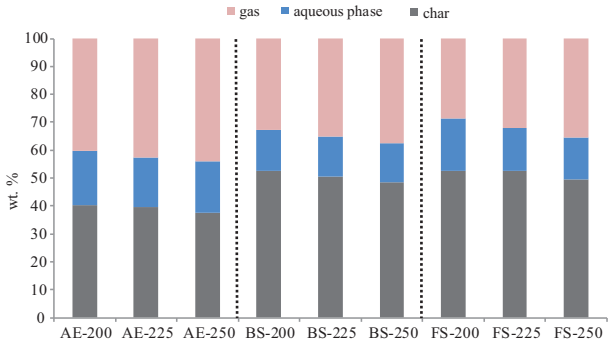

Figure 2. Carbon distribution in HTC.

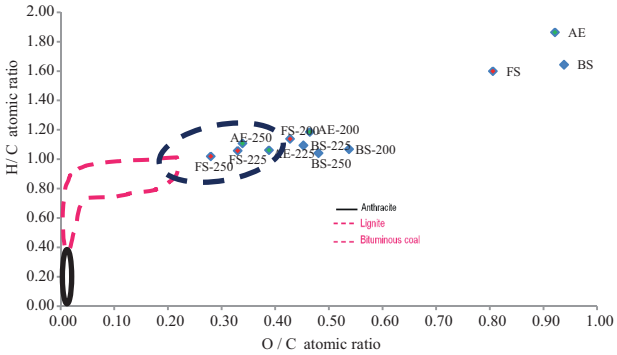

Figure 3. Atomic H/C and O/C ratios of seaweeds and its derived hydrochars (Van Kreevelen diagram).

The HTC process is a complex series of reactions including hydrolysis, dehydration, decarboxylation, demethanation, polymerization, and aromatization, simultaneously.[29] During HTC of all seaweeds, decarboxylation and dehydration reactions occurred simultaneously at all temperatures yielding hydrochars with lower O/C and H/C atomic ratios in comparison with seaweeds, which makes them more preferable as a fuel due to the decreased smoke, water vapor, and energy losses during their combustion.[26] The hydrochars derived from FS and AE at 225 and 250 °C with even lower O/C and H/C atomic ratios were found to be in the range of lignite and are expected to show better fuel characteristics. On the other hand, the hydrochars derived from BS at all temperatures were out of the range of lignite, and more similar to peat.

The variation in calorific value of hydrochars with temperature appears to be a result of the variation in their O/C ratios rather than the variation in their ash contents. Thus, in case of BS, calorific value and energy densification value (the ratio of HHV of product to HHV of raw seaweed) of hydrochar decreased with the increase of temperature from 225 to 250 °C as a result of increase in O/C ratio, even though ash content slightly decreased. In case of AE and FS, calorific values and hence energy densification values of hydrochars increased with temperature as a result of decrease in O/C ratio, although the ash content increased. Due to higher carbon content and substantially reduced ash content, the FS-derived hydrochars had the highest calorific value and resembled high quality lignite more than others. The calorific values of hydrochars, especially FS-derived hydrochars, are comparable to those of hydrochars produced from seaweeds and even lignocellulosic biomass reported in the literature.[22,23,30]

Energy yield is a practical consideration for conversion of biomass into hydrochar or biochar.[31] It shows energy efficiency of the process and was calculated by multiplying the hydrochar mass yield by the energy densification ratio. For all seaweed types, energy yield of hydrochars decreased by the increase of temperature from 225 to 250 °C due to the decreased hydrochar yield for FS and AE and due to the decreased energy densification and hydrochar yield for BS. Since lower amount of carbon in feedstock was retained in respective hydrochars during HTC of AE in comparison with those of other seaweeds, AE-derived hydrochars had the lowest energy yield.

2.4. FTIR spectra of hydrochars

FTIR spectra of seaweeds and their resulting hydrochars were taken in order to understand the changes in the chemical structure of the seaweeds during the HTC depending on the temperature. The FTIR spectra

corresponding to seaweeds and hydrochar samples are given in the Supplementary Information (Figures S1–S3). Based on the weakening of the intensity of band at 1050–1000 cm^{-1} assigned to C-O stretching of carbohydrates[32] after HTC, it can be concluded that the decomposition of carbohydrates was almost completed during HTC at highest temperature for FS. On the other hand, carbohydrates did not decompose effectively during HTC of AE and BS.

2.5. Thermal degradation behavior of seaweeds and their hydrochars under inert atmosphere

TGA of the seaweeds and hydrochars was performed to understand their pyrolytic behavior and thermal resistance (stability). Figures 4–6 show the TG/DTG profiles of seaweeds and hydrochars.

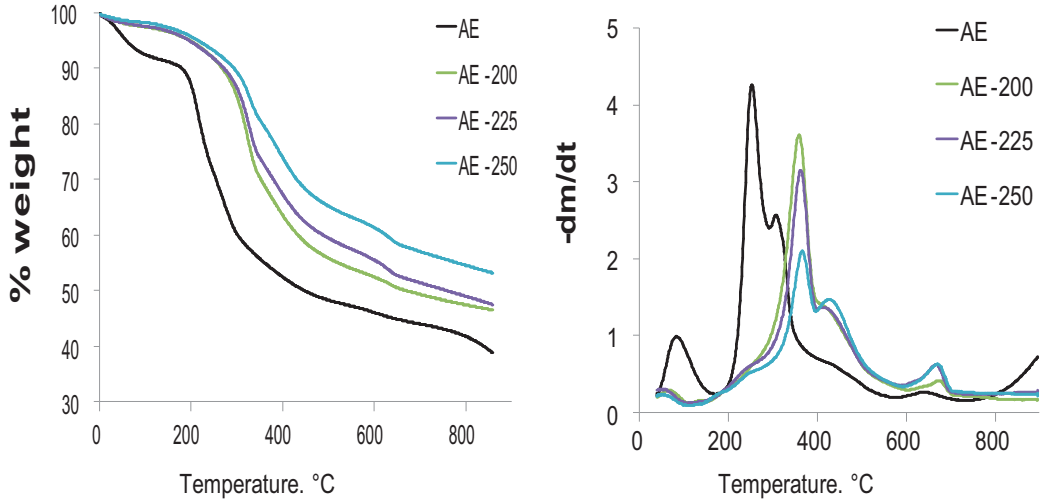

Figure 4. (a) TG curves and (b) DTG curves of AE and AE-derived hydrochars under nitrogen atmosphere.

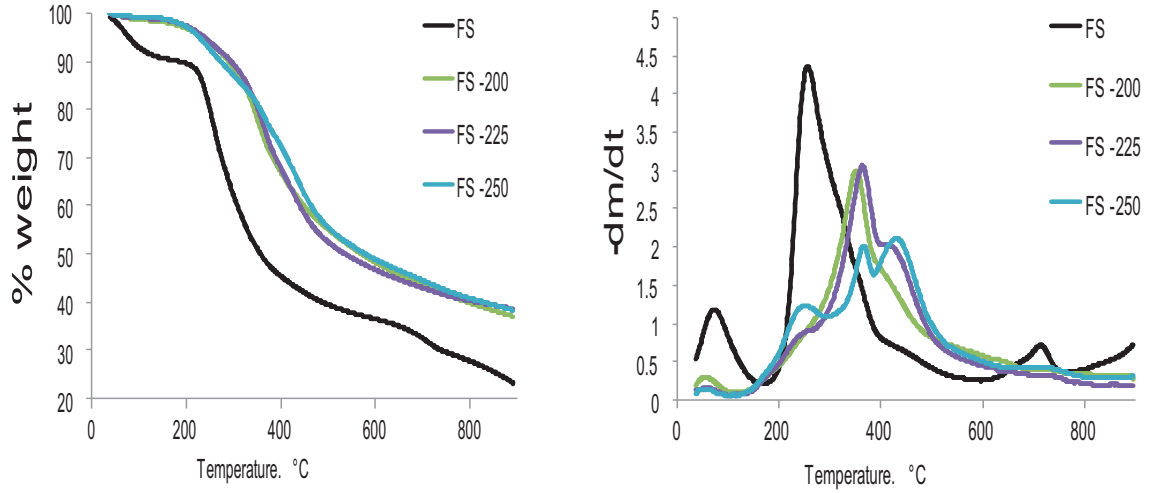

Figure 5. (a) TG curves and (b) DTG curves of FS and FS-derived hydrochars under nitrogen atmosphere.

It was inferred from the DTG curves of seaweeds that there is one main degradation stage (Figures 4–6). The peaks below 150 °C indicated the loss of the cellular and external water. The peak observed at temperatures

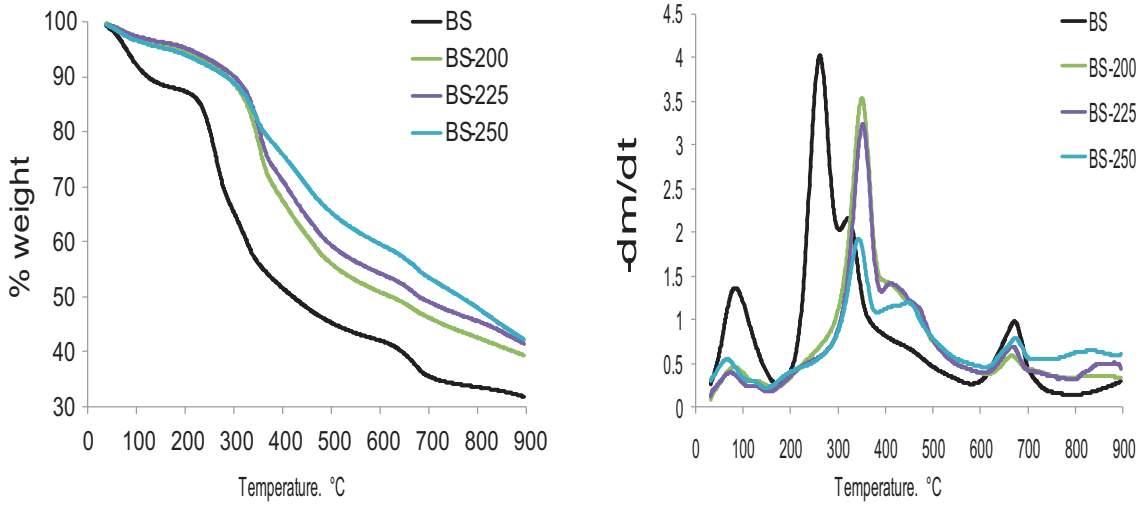

Figure 6. (a) TG curves and (b) DTG curves of BS and BS-derived hydrochars under nitrogen atmosphere.

around 600 °C indicates the decomposition of alkali carbonates. The main degradation stage included the main pyrolytic decomposition occurring over a temperature range of 150–390 °C, which is considerably lower than that of lignocellulosic biomass. In contrast to lignocellulosic biomass, seaweeds are mainly composed of carbohydrates and proteins, besides minerals. The previous study regarding the TGA experiments with different seaweed species showed that the decomposition of carbohydrate occurred at temperatures between 180 and 270 °C while the proteins decomposed at temperatures between 320 and 450 °C.[2] Based on this finding, we can say that the temperature ranges of thermal degradation of proteins and carbohydrates have overlapped in our case.

The thermal degradation behavior of seaweeds changed remarkably after HTC. DTG peak temperatures shifted to higher temperatures after HTC (Figures 4–6). This means that during HTC, even at 200 °C, all biomass was converted into a char-like product. The broad peak centered around 350 °C was attributed to the degradation of char structure. These results are in accord with the elemental analysis findings, which show that carbon and nitrogen contents increased and oxygen content decreased after HTC.

Differently, for hydrochar obtained from FS at 250 °C, a peak at around 255 °C appeared which might be attributed to the degradation of oligomeric repolymerization products formed upon hydrothermal degradation at higher temperatures.[25] It is noteworthy that the rate of the weight loss of hydrochars obtained at 250 °C was smaller than those of other hydrochars and seaweeds, suggesting that thermal stability of hydrochars is enhanced by increasing HTC temperature. This phenomenon is in line with the results shown in previous HTC studies carried out with lignocellulosic biomass.[33–35]

2.6. Combustion behavior of seaweeds and hydrochars

The aim of hydrochar production was to convert the seaweeds into a solid fuel, which would be a more appropriate feedstock in processes like combustion.[25] The main technical difficulties in combustion of biomass in boilers or power plants include higher grinding energy requirements due to poor grindability, flame instabilities due to low energy density, and difficulties in feeding biomass into combustors due to low flowability and fluidization properties.[36] TGA/DTG is known to be an effective way to analyze combustion behavior of solid fuels as stated by Toptas et al.[37] Therefore, the combustion behaviors of seaweeds and the hydrochars were investigated by thermogravimetry.

Combustion profiles of seaweeds and hydrochars are given in Figure 7 and Supplementary Information (Figure S4). In the case of raw seaweeds, the combustion processes consisted of two main stages. The first stage included formation of volatiles and their oxidation along char formation. The second stage included the oxidation of char that remained after the volatiles. The combustion profiles of seaweeds were similar to those of *Gracilaria cacalia*, *Enteromorpha clathrate*, and *Laminaria japonica* given in the literature.[38]

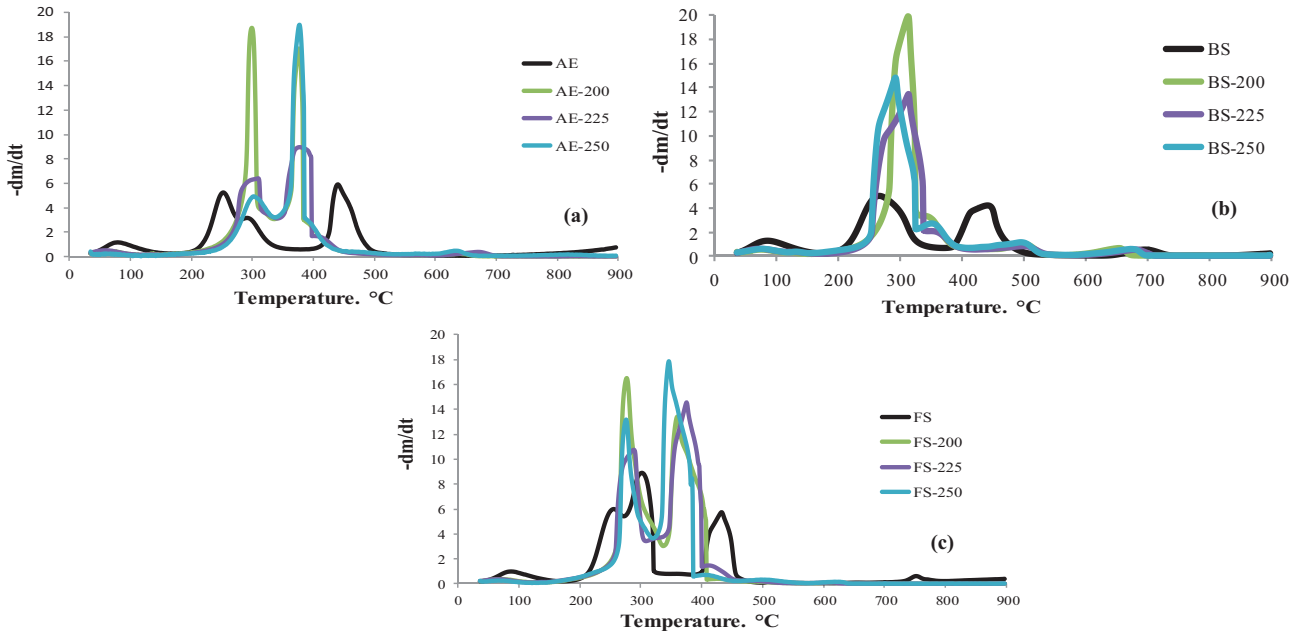

Figure 7. DTG curves of hydrochars under air atmosphere, (a) AE, (b) BS, (c) FS.

In the case of hydrochars, only one main DTG peak between 235 and 385 °C was observed for the BS-derived hydrochar; the first and second stage overlapped. However, two peaks in combustion DTG profile of the FS-derived and AE-derived hydrochars were observed. In comparison with seaweeds, first peaks moved towards higher temperatures attributing to low volatile matter in hydrochar. However, second peaks moved towards lower temperatures. This shows that char oxidation occurred easily and faster with the increase in the fixed carbon amount and homogeneity of fuel.[37] It can be stated that the fixed carbon combustion was dominant in combustion of hydrochar, while volatilization and gas-phase combustion were dominant[39] in combustion of seaweeds, which have higher volatile matter/fixed carbon ratio.

The characteristic parameters for combustion are given in Table 4. The ignition temperature was derived from the temperature where the DTG had its maximum value and the corresponding slope to the intersection with respect to the TG profile.[18] Burnout temperature was taken as the temperature where the rate of weight loss became less than 1 wt.%/min.[25] The combustion reactivity was considered to be directly proportional to the maximum combustion rate and inversely proportional to the corresponding peak temperature as stated by Miranda et al.[40] and calculated by the following equation:

$$Reactivity = 100 \times maximumcombustionrate/peaktemperature \quad (1)$$

Values, which are representatives of an average reactivity (Rm), are also given in Table 4.

Table 4. Combustion characteristics of seaweeds and hydrochars.

	Ignition temperature, °C	Burnout temperature, °C	Peak temperature, °C	Maximum combustion rate, % min^{-1}	Reactivity (% min^{-1} K^{-1})	Rm (% min^{-1} K^{-1})
AE	220	487	253; 292; 438	5.25; 3.17; 5.91	1.00; 0.56; 0.83	0.92
AE-200	277	425	299; 376	18.71;1 7.03	3.27; 2.62	2.95
AE-225	273	431	309; 377	6.41; 8.96	1.10; 1.38	1.24
AE-250	282	422	303; 378	4.93; 18.96	0.86; 2.91	1.89
BS	230	478	267; 441	4.98; 4.20	0.86; 0.59	0.73
BS-200	273	385	313	19.95	3.40	3.40
BS-225	276	386	314	13.50	2.30	2.30
BS-250	263	385	293	14.77	2.61	2.61
FS	228	456	256; 301; 432	5.99; 8.90; 5.74	1.13; 1.55; 0.81	1.15
FS-200	247	407	277; 360	16.51; 13.41	3.00; 2.11	2.55
FS-225	254	434	288; 374	10.75; 14.47	1.91; 2.24	2.08
FS-250	250	387	276; 346	13.17; 17.85	2.40; 1.10	1.75

The ignition temperature depends on how early the volatiles are released and how quickly the heat is released by combustion of volatiles as stated by Vamvuka et al.[41] Therefore, the ignition temperatures of hydrochars are higher than that of raw biomasses mainly due to the reduced content of volatiles in hydrochars and less amount of energy released by them. Peak temperatures of hydrochars in the first stage are also higher than that of raw seaweeds. A higher peak temperature may be advantageous in avoiding potential fire hazard and minimizing explosion risk in the case of using hydrochars as solid fuel as stated by Cai et al.[42] Comparison of hydrochars with seaweed revealed that HTC process lowered the burnout temperature. Therefore, hydrochars are easier to burn due to the reduced residence time or lowered temperatures to achieve complete combustion. The higher weight loss rate of char oxidation stage for hydrochars than that for seaweeds showed that HTC converted seaweeds to hydrochars which had higher reactivity as seen in Table 4. Hydrochars have also higher average reactivity (R_m) and hence better combustibility than seaweeds.

2.7. Combustion kinetics

The chemical kinetics of biomass combustion is very informative for combustion systems' design and optimization as stated by Toptas et al.[37] An integral method using dynamic analysis of the nonisothermal TGA data was utilized in order to analyze combustion kinetics of seaweeds and hydrochars. In the literature, combustion reactions are mostly assumed to be first-order chemical reactions (O_1 model) for simplification of the kinetic calculations.[37,43] However, combustion process is more complicated; it includes solid-gas phase and gas phase reactions and hence needs the utilization of different $g(\alpha)$ models in order to calculate the activation energy, E, and lnA based on the Coats–Redfern model in this study. Also, other chemical reactions (O_2 and O_3 models), boundary controlled reactions (R_2 and R_3 models), and diffusion mechanisms (D_1, D_2, D_3, and D_4 models) are employed to provide a description of the combustion reactions of seaweeds and hydrochars.[43] As described by Park et al., the form of $g(\alpha)$ that gives a straight line with the highest correlation coefficient was selected as the function of the model that best represents the kinetics of mass loss for each separate reaction.[44]

The values of E and lnA obtained from the plots of $\ln[g(\alpha)/T^2]$ against 1/T that gave the highest correlation coefficient values for all the samples are presented in Table 5. As seen from Table 5, model O_3 presented the highest correlation coefficients for all seaweeds in both devolatilization and char combustion

stages, indicating that the chemical third-order reaction is the most effective mechanism in combustion of raw seaweeds. For the BS-derived hydrochars, the main stage (overlapping devolatilization and char combustion stages) followed the third order chemical reaction mechanism. Activation energy of the main stage for the FS-derived hydrochars decreased with the increase of HTC temperature, which means combustion of char became easier as the HTC temperature increased. For the AE-derived and FS-derived hydrochars, devolatilization stage followed the three-way transport diffusion mechanism. The char combustion stage also followed the three-way transport diffusion mechanism for the AE-derived hydrochars, while it followed one-way transport diffusion mechanism for the FS-derived hydrochars. Activation energy of first stage remained in the range of 133–147 kJ mol^{-1} for the AE-derived hydrochars and in the range of 115–120 kJ mol^{-1} for the FS-derived hydrochars, which were higher than that of the raw seaweeds. As Cai et al. stated that this can be due to the decomposition of relatively reactive compounds and the release of unstable volatile matters during HTC.[42] Activation energy of the second stage increased from 76 to 93 kJ mol^{-1} for AE-derived hydrochars and from 55 to 74 kJ mol^{-1} for FS-derived hydrochars with elevation of HTC temperature. The increase of activation energy in the second stage with elevation of HTC temperature means that the combustion of char becomes harder as the HTC temperature increases due to the increase in the amount of fixed carbon.[42] Also, due to the decrease in the amount of volatiles and the increase in the amount of fixed carbon during HTC at 250 °C, a noticeable decrease of weight loss and gradually narrowed temperature intervals were observed in the first stage; the weight loss decreased remarkably to 19.3% and 26.5%, and the intervals shifted to 280–330 °C and 250–315 °C for AE and FS, respectively.

2.8. Ash composition and fouling indices of hydrochars

Table 6 lists the ash composition of seaweed-derived hydrochars as determined by X-ray fluorescence spectroscopy (XRF). All hydrochars contain predominately calcium. AE-225 has considerably higher silica content than other hydrochars. On the other hand, hydrochars have reduced alkali and alkaline earth metal content in comparison with seaweeds, except calcium (Table 2). Alkali and alkaline earth metals are effective fluxes for alumina-silicates and lower the ash fusion temperature which led to an increase in slagging and fouling tendency of seaweeds.[45] Fouling occurs in the case of partial evaporation of potassium and sodium in combination with chlorine forming alkali chlorides which condense on the surfaces of the heat exchanger. HTC of seaweeds is expected to reduce the slagging and fouling potential of resulting hydrochars due to the efficient removal of alkali metals. Therefore, various slagging and fouling indices of seaweeds and their respective hydrochars were calculated in order to predict the potential of slagging and fouling during combustion based on their mineral composition obtained by XRF analysis and presented in Table 7. The equations for alkali index (AI), acid base ratio ($R_{b/a}$), slagging (Babcock) index (SI), fouling index (FI), and slag viscosity index (SVI) are given as Eqs. (2)–(5).[24]

$$AI = \frac{Kg(Na_2O + K_2O)}{GJ}, \tag{2}$$

$$R_{B/A} = \frac{\%(Fe_2O_3 + CaO + Na_2O + K_2O + MgO)}{\%(SiO_2 + Al_2O_3 + TiO_2)}, \tag{3}$$

$$SI = \frac{\%(Fe_2O_3 + CaO + Na_2O + K_2O + MgO)}{\%(SiO_2 + Al_2O_3 + TiO_2)} * \%\,(S)\,(dry), \tag{4}$$

Table 5. Kinetic parameters obtained for combustion of seaweeds and hydrochars.

	Temperature range, °C	Weight loss (wt.%)	Reaction	E_a, kJ mol^{-1}	lnA, min^{-1}	R^2
AE	220–345	31.49	O_3^a	21.75	17.59	0.95
	376–550	23.15	O_3	80.98	14.86	0.89
AE-200	277–330	28.00	D_3^b	146.98	25.75	0.98
	330–425	37.27	D_3	75.92	10.61	0.97
AE-225	273–341	27.97	D_3	132.79	22.19	0.98
	341–431	34.78	D_3	89.66	12.94	0.96
AE-250	282–330	19.30	D_3	141.11	23.66	0.99
	330–422	37.72	D_3	93.43	13.57	0.97
BS	230–370	35.12	O_3	22.81	4.09	0.97
	385–520	23.76	O_3	105.22	19.52	0.93
BS-200	273–385	60.88	O_3	94.69	19.83	0.96
BS-225	276–410	60.02	O_3	93.41	19.49	0.95
BS-250	263–385	57.54	O_3	75.59	15.77	0.95
FS	228–360	45.39	O_3	35.56	7.17	0.97
	393–500	17.74	O_3	116.51	22.00	0.90
FS-200	247–336	39.66	D_3	115.42	18.72	0.99
	337–407	46.94	D_1^c	54.97	7.76	0.97
FS-225	254–330	31.98	D_3	117.19	19.07	0.99
	330–434	54.88	D_1	57.07	8.07	0.96
FS-250	250–316	26.49	D_3	120.66	19.81	0.99
	317–387	55.02	D_1	74.41	11.82	0.98

[a] O_3: third-order reaction-chemical reaction; [b] D_3: three-way transport-diffusion limited reaction; [c] D_1: one-way transport-diffusion limited reaction.

$$FI = \frac{\%(Fe_2O_3 + CaO + Na_2O + K_2O + MgO)}{\%(SiO_2 + Al_2O_3 + TiO_2)} * \%\,(Na_2O + K_2O)\,. \quad (5)$$

For AI, AI < 0.17 implies safe combustion, $0.17 <$ AI < 0.34 predicts probable slagging and fouling during combustion, and AI > 0.34 predicts certain slagging and fouling during combustion. In the case of $R_{b/a}$, risk of slagging is low for a value of < 0.5, while it is high to severe for a value of > 1.0 during biomass combustion. SI values of < 0.6 indicate a low slagging potential, while SI $> 0.6 <$ 2.0 indicate a medium slagging potential, and SI > 2.0 indicate a high slagging potential. For FI, a value of < 0.6 indicates a low fouling potential. $0.6 <$ FI < 40.0 indicates a medium fouling potential, and FI > 40.0 indicate high fouling potential.

AI of BS-225 and FS-225 indicates safe combustion due to the reduced Na and K contents during HTC, while that of AE-225 predicts probable slagging and fouling due to higher K content remained in hydrochar (Table 7). It should be noted that AI of hydrochars was reduced in comparison with seaweeds due to the removal of Na and K during HTC, which was partial in the case of AE. However, $R_{b/a}$ of all hydrochars predicts a high risk of slagging during their combustion which is higher for BS-225 and FS-225. Limited removal of Ca and Fe during HTC resulted in their accumulation within the char and resulted in limited decrease of $R_{b/a}$ in

Table 6. Mineral composition of hydrochar samples (g mineral/ 100 g hydrochar) by XRF spectroscopy prepared by the pressed pellet method.

	AE-225	BS-225	FS-225
Na_2O	< 0.02	< 0.02	< 0.02
MgO	< 0.01	< 0.01	< 0.01
Al_2O_3	0.32	< 0.01	< 0.01
SiO_2	2.25	0.21	0.11
P_2O_5	1.19	0.51	0.60
Cl	0.06	0.05	0.08
K_2O	0.56	0.08	0.15
CaO	5.64	9.27	3.35
TiO_2	0.18	0.01	0.02
MnO	< 0.01	0.02	0.05
Fe_2O_3	1.13	0.23	0.25
CuO	0.14	0.02	0.11

All values are dry weight %. Elements are represented as their respective oxides.

Table 7. Fouling and slagging indices of seaweeds and their respective hydrochars.

	AE	AE-225	BS	BS-225	FS	FS-225
Alkali index (AI)	7.23	0.31	3.67	0.04	3.86	0.06
Acid base ratio ($R_{b/a}$)	6.12	2.65	22.38	43.95	52.80	30.04
Slagging index (SI)	3.04	0.62	21.74	50.19	50.01	9.40
Fouling index (FI)	78.77	1.48	154.33	3.34	515.33	4.51

the cases of AE and FS and increase of $R_{b/a}$ in the case of BS. The low $R_{b/a}$ for AE-225 in comparison with other hydrochars is due to the high aluminum, silicon, and titanium content. In comparison with seaweeds, SI values of hydrochars were reduced in the cases of AE and FS and increased in case of BS. SI of AE-225 predicts a much lower slagging formation potential due to lower S content and $R_{b/a}$ value, while that of BS-225 and FS-225 predicts a high slagging formation potential when combusted. BS-225 had the highest slagging index value since it had high S content and high value of $R_{b/a}$ due to the high Ca content and low Si content. FI value predicts high fouling inclination in case of seaweeds, while it predicts medium fouling inclination due to the removal of Na and K during HTC in case of hydrochars.

3. Conclusions

HTC converted seaweeds into hydrochars with lower ash contents due to the solubility of the inorganics at subcritical water conditions. Hydrochars derived from *Fucus serratus* had the highest calorific value due to their lower ash content and higher carbon content. *Fucus serratus*- and *Alaria esculenta*-derived hydrochars became increasingly similar to lignite with higher process temperature, whereas the hydrochars derived from the mixture of *Cystoseria* sp. and *Laurencia* sp. at all temperatures were out of the range of lignite and more similar to peat. FTIR spectra of hydrochars and seaweeds revealed that decomposition of carbohydrates was almost completed during HTC of *Fucus serratus* at highest temperature, while they were not decomposed effectively

for *Alaria esculenta* and the mixture of *Cystoseria* sp. and *Laurencia* sp. The combustion analysis revealed that HTC of seaweeds modified their combustion behavior. The first peaks related with formation and oxidation of volatiles moved towards higher temperatures due to the lower volatile matter contents of hydrochars, while the second peaks related with char oxidation moved towards lower temperatures implying that char oxidation took place easily and faster due to the increased amount of fixed carbon and improved homogeneity in fuel. HTC was found to be promising in reducing the fouling potential of seaweeds from high to medium level in combustion applications.

4. Experimental

4.1. Materials

Two species of seaweeds (*Fucus serratus* and *Alaria esculenta*) were collected from the the southwest coast of Ireland, while the mixture of seaweeds, mainly consisting of *Cystoseria* sp. and *Laurencia* sp., was collected from Sinop coast in the Black Sea Region of Turkey. All seaweed samples were washed with water, dried in oven at 60 °C, and ground and sieved to a particle size of < 0.1 mm.

4.2. Hydrothermal carbonization experiments

In a typical hydrothermal carbonization experiment, a mixture of 5 g of seaweed and 20 g of deionized water (seaweed/water ratio of 25% by weight) were loaded into a 100-mL stainless steel shaking autoclave. The autoclave was then sealed and purged with nitrogen and heated to the process temperature (200–250 °C) at a rate of 5 °C min^{-1}. It was held at this temperature for 30 min. At the end of this duration, the reactor was rapidly cooled down to room temperature by immersing the reactor in ice-water. After venting the gaseous products into the atmosphere, the solid residue (hydrochar) was separated from the aqueous phase by filtration. The aqueous phase was kept in bottles for further analysis. Hydrochar was washed with distilled water (100 mL) and then dried at 105 °C for 24 h and weighed.

4.3. Feedstock and product characterization

Thermal degradation behaviors of seaweeds and hydrochar samples were investigated by a thermogravimetric analyzer (Perkin Elmer Diamond TG/DTA) under nitrogen atmosphere.

The information on proximate analysis of seaweeds and hydrochars was evaluated from their TGA plots[46] and ultimate analysis was determined by using an elemental analyzer (LECO CHNS 932) according to ASTM D3176-89.

The HHV of the feedstocks and hydrochars was calculated by the following correlation Eq. (6) proposed by Channiwala et al.:

$$HHV(MJkg^{-1}) = 0.3491 \times C + 1.1783 \times H + 0.1005 \times S - 0.1034 \times O - 0.015 \times N - 0.0211A, \quad (6)$$

where C is carbon weight percent, H is the hydrogen weight percent, S is the sulfur weight percent, O is oxygen weight percent, N is nitrogen weight percent, and A is the ash weight percent of fuels.[47] Ash composition of hydrochars was determined by XRF spectroscopy.

The protein content of seaweeds was determined using a protein analyzer (INKJEL M) and the lipid content of seaweeds was determined by hexane extraction.

The FTIR analyses of feedstocks and hydrochars were performed using attenuated total reflectance infrared spectrometer (Spectrum 100, PerkinElmer, Waltham, MA, USA). The total organic carbon (TOC) content in the aqueous phase from HTC was determined by a TOC analyzer (HachLange IL550-TOC-TN, HachLange, Loveland, CO, USA).

4.4. Combustion characteristics and kinetics

The combustion characteristics of feedstocks and hydrochars were determined by TG/DTA under air atmosphere with a flow rate of 50 mL min^{-1} and a heating rate of 20 °C min^{-1}. The combustion parameters including ignition temperature, burnout temperature, and combustion reactivity were calculated from TG/DTG plots, as described in the literature.[25,48]

Combustion kinetic analysis depended on an integral method using Coats–Redfern equation applied in dynamic analysis of the nonisothermal TG data. The process of combustion was governed by the Arrhenius law as described in Eqs. (7) and (8) below,[44]

$$\frac{d\alpha}{dt} = kf(\alpha), \tag{7}$$

$$k = A\exp\left(\frac{E}{RT}\right), \tag{8}$$

where α is the degree of conversion, t is the time, T is the temperature, A is the preexponential factor, E is the activation energy, R is the gas constant, and T is the temperature. f(α) represents the hypothetical model of the reaction mechanism.

The degree of conversion, α, is defined as,

$$\alpha = (m_0 m_t)/(m_0 m_f), \tag{9}$$

where m_0 is the initial mass of the sample, mt the mass of the sample at time t, and m_f the final mass of the sample.

For a constant heating rate β (K min^{-1}) during combustion, β = dT/dt, Eq. (7) can be written as

$$\frac{d\alpha}{f(\alpha)} = (\frac{k}{\beta}).dT. \tag{10}$$

Integrating Eq. (10) gives:

$$g(\alpha) = \int_0^{\alpha} \frac{d\alpha}{f(\alpha)} = \frac{A}{\beta}\int_{T_0}^{T} \exp\left(\frac{E}{RT}\right) dT, \tag{11}$$

where g(α) is the integral function of conversion.

Eq. (11) is integrated using the Coats–Redfern method and becomes

$$\ln\left[\frac{g(\alpha)}{T^2}\right] = ln?\left[\frac{AR}{\beta E}(1\frac{2RT}{E})\right]\frac{E}{RT}. \tag{12}$$

Plotting of ln[g(α)/T^2)] versus 1/T should give a straight line with a high correlation coefficient in the case where correct g(α) is used.[43] E can be determined from the slope –E/R, while A is calculated by taking the temperature where m_t = (m_0+ m_t)/2 as the intercept term.[37,49]

References

1. Brennan, L.; Owende, P. *Renew. Sustain. Energy Rev.* **2010**, *14*, 557-577.
2. Ross, A. B.; Jones, J. M.; Kubacki, M. L.; Bridgeman, T. *Bioresource Technol.* **2008**, *99*, 6494-6504.
3. Goh, C. S.; Lee, K. T. *Renew. Sustain. Energy Rev.* **2010**, *14*, 842-848.
4. Rengel, A. In *Proceedings of the 8th European symposium of the international farming systems association (IFSA)*, Clermont-Ferrand, France, 6-10 July 2008; Dedieu, B.; Zasser-Bedoya, S., Eds; pp. 683-692.
5. Jung, K. A.; Lim, S. R.; Kim, Y.; Park, J. M. *Bioresource Technol.* **2013**, *135*, 182-190.
6. Vanegas, C. H.; Bartlett, J. *Environ. Technol.* **2013**, *34*, 2277-2283.
7. Anastasakis, K.; Ross, A. B. *Bioresource Technol.* **2011**, *102*, 4876-4883.
8. Libra, J. A.; Ro, K. S.; Kammann, C.; Funke, A.; Berge, N. D.; Neubauer, Y.; Titirici, M. M.; Fühner, C.; Bens, O.; Kern, J. et al. *Biofuels* **2011**, *2*, 71-106.
9. Xu, Q.; Qian, Q.; Quek, A.; Ai, N.; Zeng, G.; Wang, J. *ACS Sustainable Chem. Eng.* **2013**, *1*, 1092-1101.
10. Kruse, A.; Funke, A.; Titirici, M. M.. *Curr. Opin. Chem. Biol.* **2013**, *17*, 515-521.
11. Liu, F.; Yu, R.; Guo, M. *J. Mater. Sci* **2017**, *52*, 1736-1746.
12. Guo, S.; Dong, X.; Wu, T.; Zhu, C. *Energy Convers. Manag.* **2016**, *123*, 95-103.
13. Parshetti, G. K.; Chowdhury, S.; Balasubramanian, R. *Bioresource Technol.* **2014**, *161*, 310-319.
14. Broch, A.; Jena, U.; Hoekman, S. K.; Langford, J. *Energies* **2014**, *7*, 62-79.
15. Koottatep, T.; Fakkaew, K.; Tajai, N.; Pradeep, S. V.; Polprasert, C. *Renew. Energ.* **2016**, *99*, 978-985.
16. Fakkaew, K.; Koottatep, T.; Puassayanavin, T.; Polprasert, C. *J. Water Sanit. Hyg. Dev.* **2015**, *5*, 439-447.
17. Danso-Boateng, E.; Shama, G.; Wheatley, A. D.; Martin, S. J.; Holdich, R. G. *Bioresource Technol.* **2015**, *177*, 318-327.
18. He, C.; Giannis, A.; Wang, J.-Y. *Appl.Energy* **2013**, *111*, 257-266.
19. Kantarli, I. C.; Kabadayi, A.; Ucar, S.; Yanık, J. *Waste Manage.* **2016**, *56*, 530-539.
20. Reza, M. T.; Freitas, A.; Yang, X.; Hiibel, S.; Lin, H.; Coronella, C. J. *Environ. Prog. Sustainable Energy* **2016**, *35*, 1002-1011.
21. Oliveira, I.; Blöhse, D.; Ramke, H. G. *Bioresource Technol.* **2013**, *142*, 138-146.
22. Xu, Q.; Qian, Q.; Quek, A.; Ai, N.; Zeng, G.; Wang, J. *ACS Sustain. Chem. Eng.* **2013**, *1*, 1092-1101.
23. Smith, A. M.; Ross, A. B. *Algal Res.* **2016**, *16*, 1-11
24. Smith, A. M.; Singh, S.; Ross, A. B. *Fuel* **2016**, *169*, 135-145.
25. Pala, M.; Kantarli, I. C.; Buyukisik, H. B.; Yanik, J. *Bioresource Technol.* **2014**, *161*, 255-262.
26. Chen, J.; Chen, Z.; Wang, C.; Li, X. *Mater. Lett.* **2012**, *67*, 365-368.
27. Liu, Z.; Quek, A.; Hoekman, S.K.; Balasubramanian, R. *Fuel* **2013**, *103*, 943-949.
28. Missaoui, A.; Bostyn, S.; Belandria, V.; Cagnon, B.; Sarh, B.; Gökalp, I. *J. Anal. Appl. Pyrolysis* **2017**, *128*, 281-290.
29. Xiao, L.P.; Shi, Z. J.; Xu, F.; Sun, R.C. *Bioresource Technol.* **2012**, *118*, 619-623.
30. Hoekman, S.; Broch, A.; Robbins, C. *Energ. Fuel,* **2011**, *25*, 1802-1810.
31. Lynam, J.; Reza, M. T.; Yan, W.; Vásquez, V.; Coronella, C., *Biomass Convers. Biorefin.* **2015**, *5*, 173-181.
32. Wiercigroch, E.; Szafraniec, E.; Czamara, K.; Pacia, M. Z.; Majzner, K.; Kochan, K.; Kaczor, A.; Baranska, M.; Malek, K. *Spectrochim. Acta A* **2017**, *185*, 317-335.
33. Guo, S.; Dong, X.; Zhu, C.; Han, Y.; Ma, F.; Wu, T. *Bioresource Technol.* **2017**, *233*, 92-98.
34. Kim, K. H.; Kim, J.; Cho, T.; Choi, J. W. *Bioresource Technol.* **2012**, *118*, 158-162.

35. Volpe, M.; Fiori, L. *J. Anal. Appl.Pyrol.* **2017**, *124*, 63-72.
36. Sarvaramini, A.; Assima, G.P.; Beaudoin, G.; Larachi, F. *Fuel* **2014**, *115*, 749-757.
37. Toptas, A.; Yildirim, Y.; Duman, G.; Yanik, J. *Bioresource Technol.* **2015**, *177*, 328-336.
38. Yu, L. J.; Wang, S.; Jiang, X. M.; Wang, N.; Zhang, C. Q. *J. Ther. Anal.Calor.* **2008**, *93*, 611-617.
39. Malika, A.; Mohammed, A.; Guhel, Y. *Waste Biomass Valor.* **2017**, https://doi.org/10.1007/s12649-017-0128-2
40. Miranda, M. T.; Arranz, J. I.; Román, S.; Rojas, S.; Montero, I.; López, M.; Cruz, J. A. *Fuel Process. Technol.* **2011**, *92*, 278-283.
41. Vamvuka, D.; Sfakiotakis, S. *Thermochimica Acta* **2011**, *526*, 192-199.
42. Cai, J.; Li, B.; Chen, C.; Wang, J.; Zhao, M.; Zhang, K. *Bioresource Technol.* **2016**, *220*, 305-311.
43. Gil, M.V.; Casal, D.; Pevida, C.; Pis, J. J.; Rubiera, F. *Bioresource Technol.* **2010,** *101*, 5601-5608
44. Park, S. W.; Jang, C. H. *Energy* **2012**, *39*, 187-195.
45. Munir, S.; Nimmo, W.; Gibbs, B. M. *Fuel* **2011**, *90*, 126-135
46. Pazó, J.A.; Granada, E.; Saavedra, Á.; Eguía, P.; Collazo, J. *Int. J. Mol. Sci.* **2010**, *11*, 2701-2714.
47. Channiwala, S. A.; Parikh, P.P. *Fuel* **2002**, *81*, 1051-1063.
48. Xiang-guo, L.; Bao-guo, M.; Li, Xu.; Zhen-wu, H.; Xin-gang, W. *Thermochim. Acta* **2006**, *441*, 79-83.
49. Zhou, L.; Wang, Y.; Huang, Q.; Cai, J. *Fuel Process. Technol.* **2006**, *87*, 963-969.

Supplementary Information (SI)

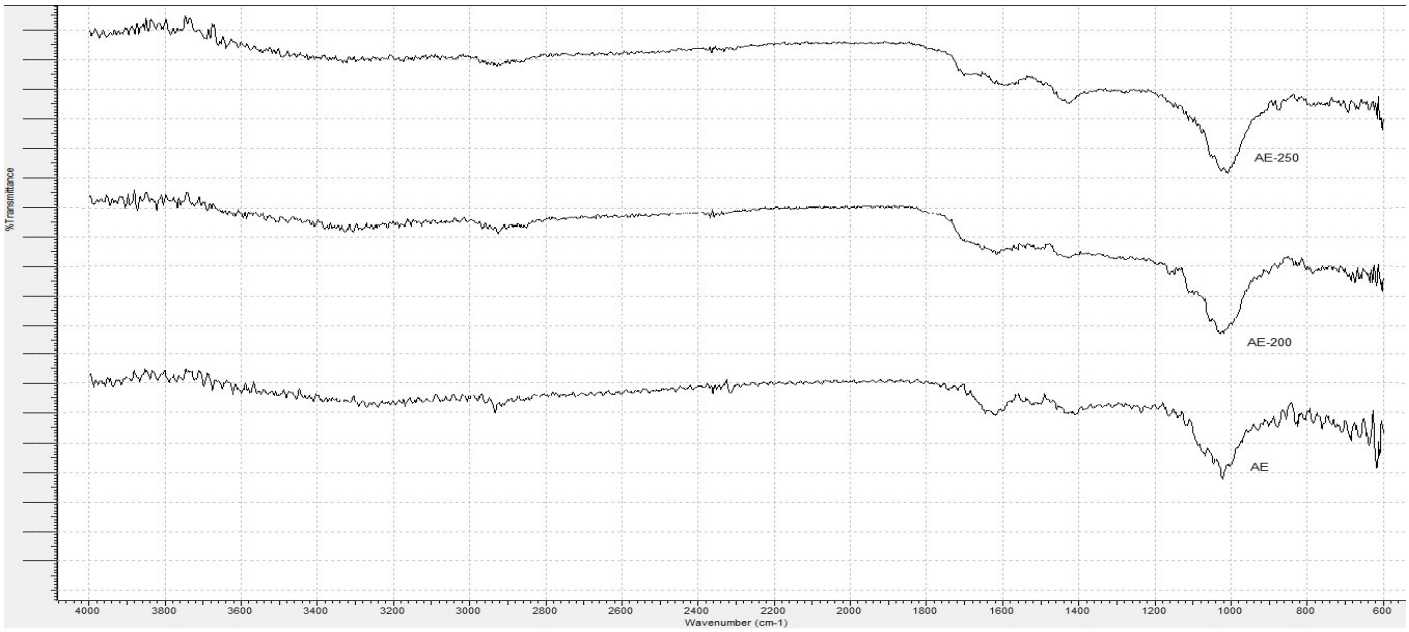

Figure S1. FTIR spectra of AE and AE-derived hydrochars.

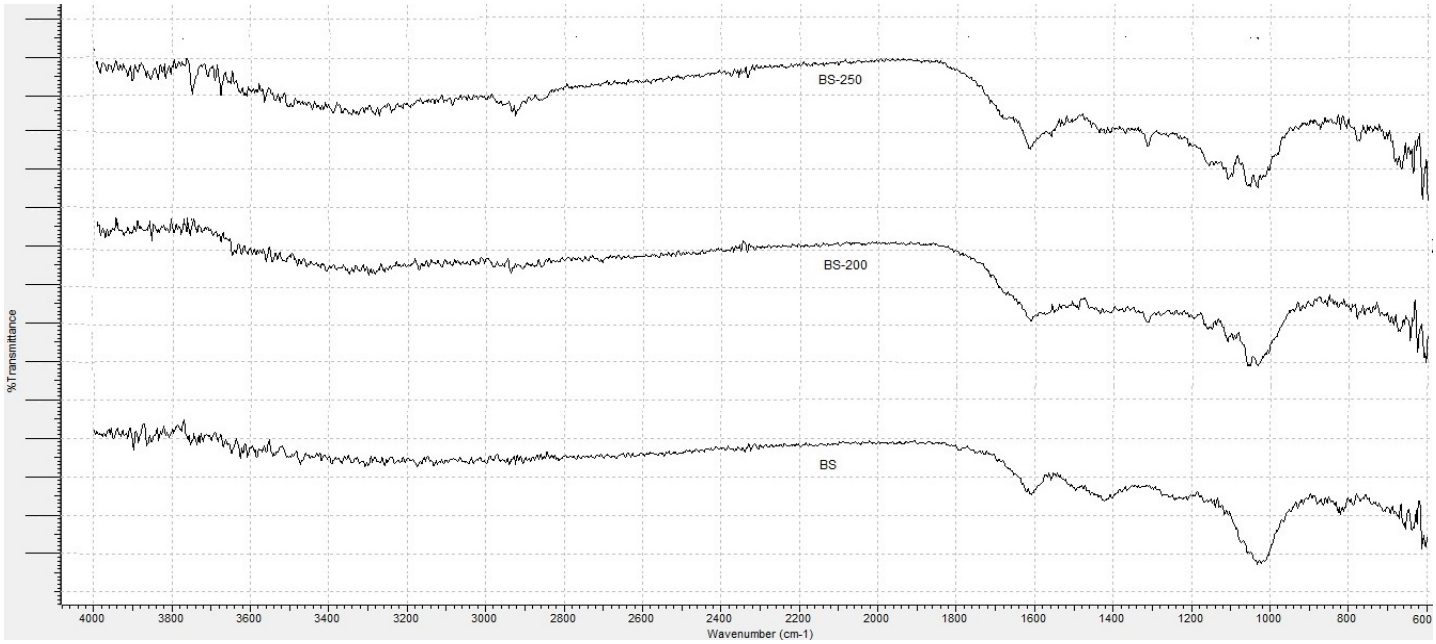

Figure S2. FTIR spectra of BS and BS-derived hydrochars.

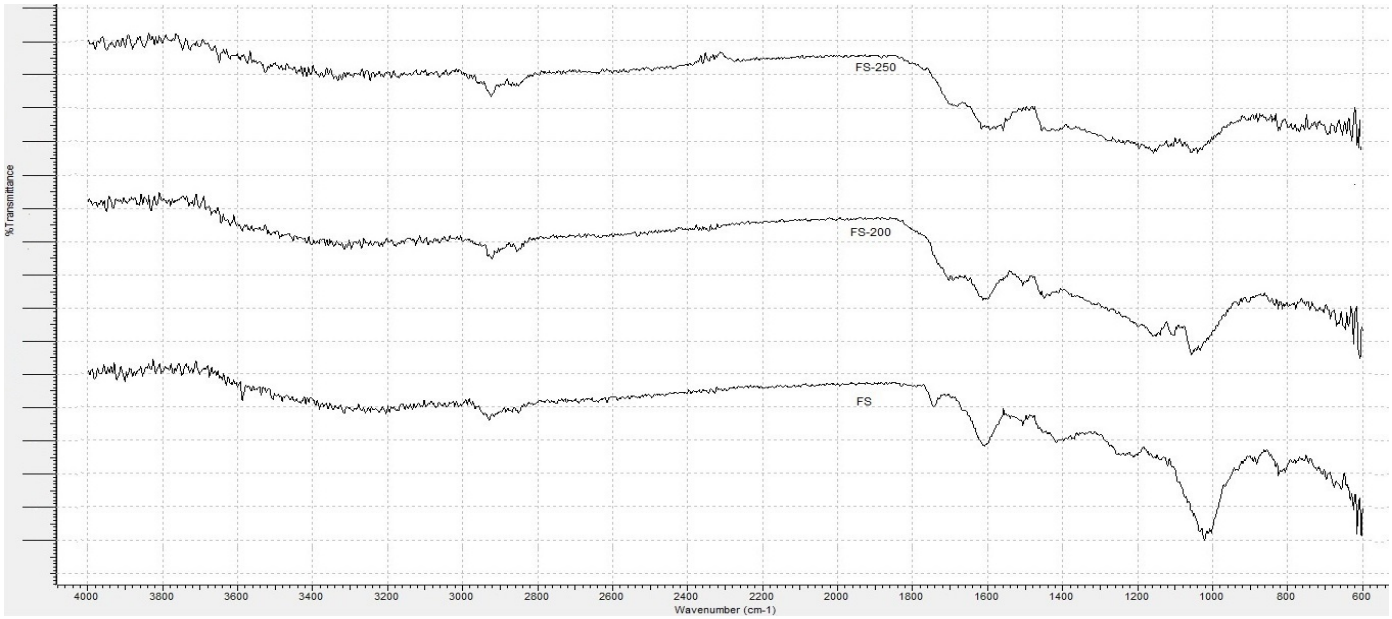

Figure S3. FTIR spectra of FS and FS-derived hydrochars.

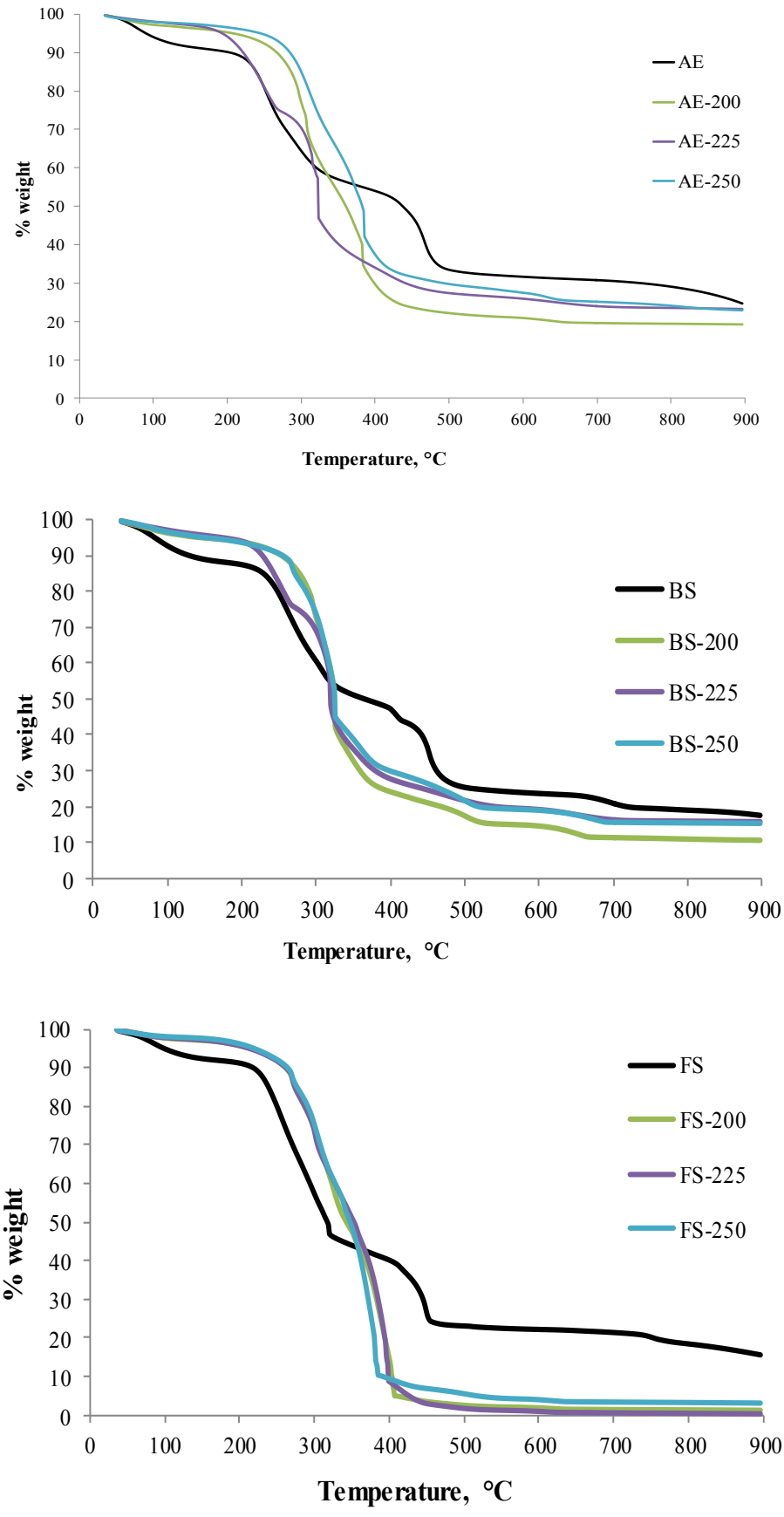

Figure S4. TG curves of seaweeds and seaweed-derived biochars.